

## Fe<sub>2</sub>O<sub>3</sub> Nanorods Grown on Reduced Graphite Oxide for the Anode of Lithium Ion battery

Jinlong Zuo<sup>1, a</sup>, Ruifeng E<sup>1, b</sup>, Junsheng Li<sup>1, c</sup>, Zhi Xia<sup>1, d</sup>, Xuewei Wang<sup>1, e</sup>, and Xinguo Yang<sup>1, f</sup>

<sup>1</sup> Harbin University of Commerce, Harbin 150076, China;

<sup>a</sup>mdjzjl@163.com, <sup>b</sup>450536651@qq.com, <sup>c</sup>3882751@qq.com, <sup>d</sup>275209599@qq.com, <sup>e</sup>827127137@ccc.com, <sup>f</sup>525348049@qq.com

**Keywords:** Fe<sub>2</sub>O<sub>3</sub>, GO, anode, LIB.

**Abstract.** Fe<sub>2</sub>O<sub>3</sub> nanorods grown on reduced graphite oxide (RGO) was synthesized via a facile hydrothermal method followed by a heat-treatment process. The Fe<sub>2</sub>O<sub>3</sub> nanorods grown on the RGO has a average diameter of 40 nm, which is smaller than the pure Fe<sub>2</sub>O<sub>3</sub> nanorod. Investigated as an anode material for Li-ion batteries, the composites exhibits a stable and reversible capacity of over 1000mAh g<sup>-1</sup> and better cycle performance than Fe<sub>2</sub>O<sub>3</sub> nanorods. The improving performance may because that the structure provides a short path for lithium-ion diffusion and effective accommodation of the strain generated from volume expansion during the lithiation/delithiation process.

### Introduction

The rechargeable Li-ion battery (LIB) has attracted intensive research interest because of its broad applications in energy storage devices for electric, hybrid electric vehicles, and intermittent renewable energy sources due to their high energy and power densities and long cycle lifetime.<sup>[1]</sup> In order to satisfy the requirements of application, exploring new electrode materials with high capacity and excellent stability is crucial for high-performance LIBs.<sup>[2-4]</sup> Nowadays, one major challenge in the development of LIBs is to find safe and cheap anode materials with large reversible capacity, good rate capability, and well cycle performance.<sup>[5,6]</sup> As the commercial anode material used, graphite has some disadvantages that limit its application, including low specific capacity (theoretical capacity of 372 mAh g<sup>-1</sup>) and poor rate performance.<sup>[7]</sup> Thus, it is imperative to develop new anode materials with enhanced Li<sup>+</sup> storage performance and large capacity.

In recent years, transition metal composites have been studied as the electrode materials due to their chemical stability, low cost and being environmental friendly. Metal oxides, sulfides and their composites with various morphologies were demonstrated with desired performance as the anodes of Li ion battery, such as Fe<sub>2</sub>O<sub>3</sub>, Co<sub>3</sub>O<sub>4</sub>, SnO<sub>2</sub>, NiS, MoS, etc.

Recently, iron oxides have received increased attention as a promising anode materials for rechargeable lithium-ion batteries due to their high theoretical capacity  $\approx 1000 \text{ mA h g}^{-1}$ , non-toxicity, high abundance, and low processing cost. Fe<sub>2</sub>O<sub>3</sub> with nanoparticles, nanosheets and some other structures have been studied. However, Fe<sub>2</sub>O<sub>3</sub> suffer from huge volume change during the charge/discharge progress, which is unfavourable for the performance of anode material for LIB. Moreover, the low conductivity of iron oxides also induces performance degradation, particularly when charging and discharging at high current densities. In order to alleviate the large volume variation problem and to increase the electronic conductivity, carbon coatings have been extensively explored.

Herein, we report a facile measure to fabricate a Fe<sub>2</sub>O<sub>3</sub> nanorods grown on reduced graphite oxide (Fe<sub>2</sub>O<sub>3</sub>-RGO), via a simple hydrothermal method followed by a heat-treatment process. Without the surfactant, the Fe<sub>2</sub>O<sub>3</sub> nanorods uniformly grown on the surface of RGO. Investigated as an anode material for Li-ion batteries, the composites exhibits a stable and reversible capacity of over 1000mAh g<sup>-1</sup> and better cycle performance than Fe<sub>2</sub>O<sub>3</sub> nanorods.

## Experiment Section

### Synthesis of Fe<sub>2</sub>O<sub>3</sub>-RGO composite.

In a typical synthesis, 2 mmol FeCl<sub>3</sub>·9H<sub>2</sub>O were dissolved in 18 mL of distilled H<sub>2</sub>O. The precursor solution was magnetically stirred for 2h. Afterwards, 20 mL 1 g L<sup>-1</sup> graphene oxide (GO) aqueous was added into the above solution and then ultrasonicated for 1h (GO were synthesized by a modified Hummers method). The above solution was transferred into a Teflon-lined autoclave, sealed, and maintained at 180 °C for 10 h. After cooling to room temperature naturally, the resulting black solid products were collected after centrifugation, washing and drying. Subsequently, the above resulting black solid was heated treating at 800 °C under N<sub>2</sub> for 2 h and the Fe<sub>2</sub>O<sub>3</sub>-RGO composite could be obtained. For comparison, Fe<sub>2</sub>O<sub>3</sub> nanorod were fabricated by the similar treatment without adding GO.

### Characterizations.

X-ray diffraction (XRD) analyses of all samples were performed in the range 10-80° (2θ) on a Bruker D8 Advance diffractometer equipped with Cu Kα (λ = 1.5406 Å) radiation and a LynxEye Detector. The accelerating voltage and the applied current were 40 kV and 20mA. The morphologies were characterized by transmission electron microscopy. The surface morphologies were observed by scanning electron microscopy (SEM) images that recorded with a Hitachi S-4800 field emission scanning electron microscope operating at 15 kV. The samples were outgassed for 10 h at 150 °C under vacuum before the measurements.

### Electrochemical measurements.

The electrochemical performances were evaluated under the same conditions using coin-type half cells. The working electrodes were prepared by pasting a mixture of 80 wt % active materials, 10 wt % super-P carbon black and 10 wt % polyvinylidene fluorides (PVDF) were mixed into N-methyl-2-pyrrolidinone (NMP). The obtained slurry was cast onto a copper foil and dried in vacuum at 100 °C for 10 h to remove excess solvent. The active materials loaded on the electrode were about 1.0-1.5 mg cm<sup>-2</sup>. Electrochemical measurements were carried out on coin-type cells with lithium metal as the counter/reference electrode, Cellgard 2400 membrane as the separator, and the electrolyte solution obtained by dissolving 1 M LiPF<sub>6</sub> into EC : EMC : DMC = 1 : 1 : 1 organic solutions. CR2025 coin cells were assembled in Ar ambient filled glovebox. Charge-discharge cycles of the half-cells were evaluated in the range of 0.01-3 V vs Li<sup>+</sup>/Li at room temperature using LAND CT2001A model battery test system (Wuhan Jinnuo Electronics, Ltd.) under constant current condition. For electrode, all the specific capacities reported and current densities used were based on the total weight of the nanocomposite. Cyclic Voltammetry (CV) was performed using Princeton Versa STAT 3 at a scanning rate of 0.1 mV s<sup>-1</sup> in the range of 0.01-3 V (vs. Li<sup>+</sup>/Li). Electrochemical impedance spectroscopy (EIS) was taken using Versa STAT 3 with the frequency ranging from 10 kHz to 10 mHz and an AC signal of 5 mV in amplitude as the perturbation.

## Results and Discussion

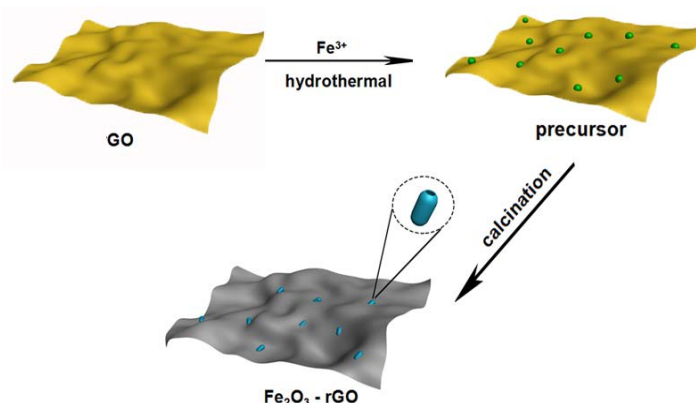


Figure 1. Formation process of Fe<sub>2</sub>O<sub>3</sub>-rGO composites

The formation progress is shown in Figure 1. Firstly,  $\text{Fe}^{3+}$  were absorbed to the function groups (  $-\text{COOH}$  and  $-\text{OH}$  ) of the graphene oxide. In the sequence hydrothermal progress, the  $\text{Fe}_2\text{O}_3$  precursor gradually formed on the surface of the GO. Then, through the calcination, the  $\text{Fe}_2\text{O}_3$  nanorods structure was obtained, and crystallized. Meanwhile, the GO was reduced to RGO. The crystallographic structures of  $\text{Fe}_2\text{O}_3$  nanorod and  $\text{Fe}_2\text{O}_3$ -RGO were analyzed by X-ray powder diffraction (XRD) shown in Figure 2. The characteristic peaks observed at  $2\theta = 24.1, 33.2, 35.6,$  and  $64.0$  were corresponding to the (012), (104), (110), and (300) planes of  $\text{Fe}_2\text{O}_3$  respectively, which indexed to the standard hematite (PDF 33-0664). The characteristic (002) peak of carbon was shadowed by the (012) peak of  $\text{Fe}_2\text{O}_3$  crystals at the similar degree. In order to investigate the carbon in the composite, Raman spectrum was shown in Figure 3, which indicates a D-band at  $1341\text{ cm}^{-1}$  and a G-band at  $1595\text{ cm}^{-1}$  for carbon in  $\text{Fe}_2\text{O}_3$ -RGO composite. The peaks below  $1000$  in  $\text{Fe}_2\text{O}_3$  and  $\text{Fe}_2\text{O}_3$ -RGO are corresponding to  $\text{Fe}_2\text{O}_3$ .

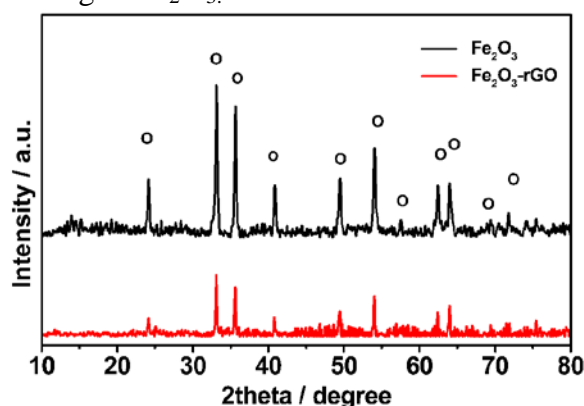


Figure 2. XRD pattern of  $\text{Fe}_2\text{O}_3$  and  $\text{Fe}_2\text{O}_3$ -rGO composites

The microstructure of the sample is revealed by SEM shown in Figure 4. It can be seen that in Figure 4b and 4c  $\text{Fe}_2\text{O}_3$  rods were uniformly grown on the surface of the RGO to form a 3D structure, which is favorable for the transformation of  $\text{Li}^+$ . Without the addition of GO, the pure  $\text{Fe}_2\text{O}_3$  shown in Figure 4a has a hollow-rod structure with a size of  $400\text{ nm}$  in length. However, the  $\text{Fe}_2\text{O}_3$  in the composite was about  $100\text{ nm}$  in length much smaller than that of  $\text{Fe}_2\text{O}_3$  rod, which may be as the consequence that the wrap of RGO may restrict the growth of it.

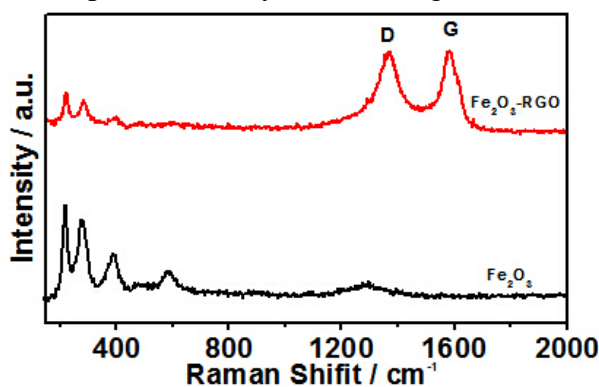


Figure 3. Raman spectrum of  $\text{Fe}_2\text{O}_3$  and  $\text{Fe}_2\text{O}_3$ -rGO composites

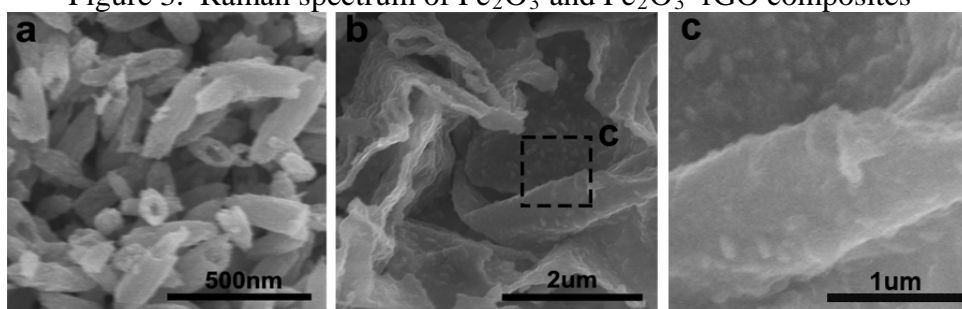


Figure 4. SEM images of  $\text{Fe}_2\text{O}_3$  (a),  $\text{Fe}_2\text{O}_3$ -rGO composites (b) and magnified(c)

The electrochemical performance of the as-synthesized Fe<sub>2</sub>O<sub>3</sub>-RGO was evaluated by assembling the architecture in a CR2025 coin cell as the anode. The voltage profile vs Li<sup>+</sup>/Li at 100 mA g<sup>-1</sup> rate between 0.01 and 3 V was shown in Figure 5. The discharge and charge capacities of the first cycle for Fe<sub>2</sub>O<sub>3</sub>-RGO electrode were 1005.8 mAh g<sup>-1</sup> and 996.1 mAh g<sup>-1</sup>, respectively. After 10 cycle, the discharge capacity was 900 mAh g<sup>-1</sup> with a retention rate of 90%, which is higher than that of the Fe<sub>2</sub>O<sub>3</sub> rods.

Based on the above analyses, the Fe<sub>2</sub>O<sub>3</sub>-RGO composite electrode displays excellent electrochemical performance, which should be attributed to their distinct structure that offer the following benefits: (1) The 3D networks comprised by Fe<sub>2</sub>O<sub>3</sub> and RGO provides a large amount of available surface sites for Li<sup>+</sup> ions insertion, which is favorable for the physical contact with the electrolyte and could provide rapid Li<sup>+</sup> ion transport channels. (2) The RGO layer on the Fe<sub>2</sub>O<sub>3</sub> surface in the composite are beneficial for the fast transfer of electrons. It is concluded that the synergetic effect among Fe<sub>2</sub>O<sub>3</sub> nanorods and RGO is responsible for the excellent lithium storage performance of the Fe<sub>2</sub>O<sub>3</sub>-RGO electrode.

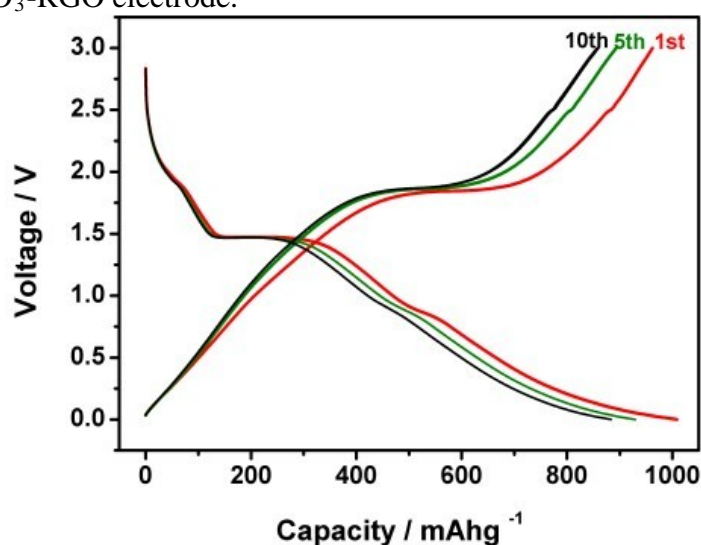


Figure 5. Charge and discharge spectra of Fe<sub>2</sub>O<sub>3</sub> and Fe<sub>2</sub>O<sub>3</sub>-rGO composites

## Conclusion

In summary, we have successfully synthesized an Fe<sub>2</sub>O<sub>3</sub>-RGO composite via a facile hydrothermal method followed by a calcination process. Investigated as an anode material for Li-ion batteries, the composites exhibits a stable and reversible capacity of over 1000mAh g<sup>-1</sup> and better cycle performance than Fe<sub>2</sub>O<sub>3</sub> nanorods. The excellent performance of the electrode can be attributed to the small diameter elongated nanostructure that provides a short diffusion path for lithium-ion diffusion and also accommodates the strain generated during the lithiation/ delithiation process.

## Acknowledgment

This research is financially supported by Natural Science Foundation of Heilongjiang Province of China (NO. E201355).

## References

- [1] P. Poizot, S. Laruelle, S. Grugeon, L. Dupont, J. M. Tarascon, *Nature* 2000 , 407 , 496.
- [2] A. S. Arico, P. Bruce, B. Scrosati, J. M. Tarascon, W. Van Schalkwijk, *Nat. Mater.* 2005, 4, 366 .
- [3] M. Armand, J. M. Tarascon, *Nature* 2008, 451, 652.
- [4] M. G. Kim, J. Cho, *Adv. Funct. Mater.* 2009, 19, 1497.

- [5] X. W. Lou, D. Deng, J. Y. Lee, J. Feng, L. A. Archer, *Adv. Mater.* 2008, 20, 258.
- [6] Z. Y. Yin, J. X. Zhu, Q. Y. He, X. H. Cao, C. Tan, H. Y. Chen, Q. Y. Yan, H. Zhang, *Adv. Energy Mater.* 2014, 4, 1300574.
- [7] W. Xu, J. Wang, F. Ding, X. Chen, E. Nasybulin, Y. Zhang, J. G. Zhang, *Energy Environ. Sci.* 2014, 7, 513.